Hindawi Publishing Corporation
International Journal of Chemical Engineering
Volume 2015, Article ID 874340, 7 pages
http://dx.doi.org/10.1155/2015/874340

Research Article

Synthesis, Characterization, and Thermal Decomposition Kinetics of Manganese Complex of Methionine Hydroxy Analogue

Mei-Ling Wang, Zhi-Xian Wu, Qing Zang, and Guo-Qing Zhong

School of Material Science and Engineering, Southwest University of Science and Technology, Mianyang 621010, China

Correspondence should be addressed to Guo-Qing Zhong; zgq316@163.com

Received 20 July 2015; Revised 8 September 2015; Accepted 10 September 2015

Academic Editor: Donald L. Feke

The manganese complex of methionine hydroxy analogue was synthesized with methionine hydroxy analogue and manganese chloride as main raw materials. The composition and structure of the complex were characterized by elemental analyses, infrared spectra, and X-ray powder diffraction. The formula of the complex was $Mn(C_5H_9O_3S)_2$. The experimental results indicated that the manganese ion was, respectively, coordinated by the carboxylic and hydroxyl oxygen atoms from the methionine hydroxy analogue ligand. The crystal structure of the complex belonged to monoclinic system with the lattice parameters of $a = 1.2775$ nm, $b = 1.5764$ nm, $c = 1.5764$ nm, and $\beta = 94.06^\circ$. The thermal decomposition process of the complex was studied by thermogravimetry and differential thermal analysis. The decomposition of the complex has taken place above 200°C. The residue was mainly manganese sulfide, and the experimental and calculated percentage mass loss was also given. The parameters of thermal decomposition kinetics for the complex, such as activation energy, reaction order, and preexponential factor, were calculated by using Kissinger, Flynn-Wall-Ozawa, and Freeman-Carroll methods, and the kinetic equations of the thermal decomposition were obtained.

1. Introduction

DL-2-Hydroxy-(4-methylthio) butanoic acid, which is known as methionine hydroxy analogue (abbreviated as H_2MHA), is equivalent to methionine in biological value. In the digestive tract, the complexes of H_2MHA are absorbed by the amino acid pathway, and the absorption speed is fast and the absorption rate is high [1]. The complexes of methionine hydroxy analogue can be used as feed additives, which can provide the essential trace elements and methionine sources for animal growth, and these complexes have the advantages of stable chemical properties, nontoxicity, little stimulation to animals, small side effects, and so on [2]. Many forms of metal complexes with amino acids and hydrolysed proteins, less commonly, with other organic ligands molecules are commercially available. The functions of the complexes of H_2MHA are similar to that of the complexes of natural amino acid and trace elements, while they are easier to meet the needs of the market than the complexes of natural amino acid and trace elements [3, 4]. So far, the complexes of H_2MHA have been rarely reported [5–7], especially in the thermal decomposition mechanism and the thermal decomposition kinetics of the complexes of H_2MHA. Here we report the synthesis, characterization, and thermal decomposition mechanism of a manganese complex of H_2MHA, and the thermal decomposition kinetic parameters of the complex are studied by using three different methods. These results can provide reliable scientific basis for the further research and the development of new products.

2. Experimental

2.1. Materials and Physical Measurements. All chemicals purchased were of analytical reagent grade and used without further purification. Methionine hydroxy analogue (industrial product with water content of 12%) was provided by Xingjia Bio-Engineering Co., Ltd., Changsha, and manganese chloride tetrahydrate was purchased from Sinopharm Chemical Reagent Co., Ltd., Shanghai.

The elemental analyses for C, H, S, and O in the complex were measured on a Vario EL CUBE elemental analyzer, and the content of manganese was determined by EDTA complexometric titration with eriochrome black T as indicator. The IR spectrum was obtained with KBr pellets on a Nicolet 5700 FTIR spectrophotometer in the range of 4000–400 cm^{-1}. The powder X-ray diffraction (XRD) pattern of the complex was recorded by a D/max-II X-ray diffractometer with Cu $K_{\alpha 1}$ radiation and Ni filter, voltage of 35 kV, current of 60 mA, and scanning speed of 8° min^{-1} at room temperature, and the XRD data were collected in the diffraction angle range of 3–80°. The thermal analysis data of the complex were obtained by using a SDT Q600 thermogravimetry analyzer in the air atmosphere from room temperature to 600°C, and the test sample mass was about 3.5 mg.

2.2. Synthesis of $Mn(HMHA)_2$. 88% of methionine hydroxy analogue (20 mmol, 3.41 g) and manganese chloride tetrahydrate (10 mmol, 1.98 g) were weighed and mixed in a beaker and heated to dissolve completely. The solution of sodium hydroxide (20 mmol, 0.80 g) was added to the above solution by drops under stirring. The pH of the solution was 6-7 after adding, and no precipitation was generated. Continue to heat with stirring until the solution was concentrated to about 10 mL, then the pink precipitation was generated, and the pH of the solution was about 6. After the solution cooling, the resultant was separated from the reaction mixture by filtration and washed by a small amount of anhydrous ethanol. The resultant was placed in a silica gel desiccator for 1 week. The product was pink powder (2.74 g) and the yield was about 77.6%.

3. Results and Discussion

3.1. Composition and Property. The results of elemental analyses for the complex are shown in Table 1. The experimental results coincide with the theoretical calculation, and the molecular formula of the complex is $Mn(C_5H_9O_3S)_2$ (M_r = 353.30); namely, its composition is $Mn(HMHA)_2$. The solid complex is stable in the air, easily dissolved in water, and not easy to absorb moisture.

3.2. X-Ray Powder Diffraction Analysis. The XRD pattern of the complex is shown in Figure 1. The background of the XRD pattern is small and the diffractive intensity is strong, and the result indicates that the complex has a fine crystalline state. The index calculation of the XRD data is based on the computer programs of least squares method [8, 9], and the calculated results are shown in Table 2. As Table 2 shows, all the diffraction data can be very well indexed by a set of cell parameters according to monoclinic system, the calculated spacing values d_{cal} are consistent with the experimental spacing values d_{exp}, and the maximum relative error is less than 0.3%. The result indicates that the complex is a single phase compound and the crystal structure of the complex belongs to the monoclinic system with the lattice parameters of a = 1.2775 nm, b = 1.5764 nm, c = 1.5764 nm, and β = 94.06°.

Table 1: Elemental analysis data of the complex $Mn(HMHA)_2$.

Element	Mn	C	H	S	O
Experimental result/%	15.86	34.05	5.37	17.93	26.79
Calculated result/%	15.55	33.99	5.14	18.15	27.17

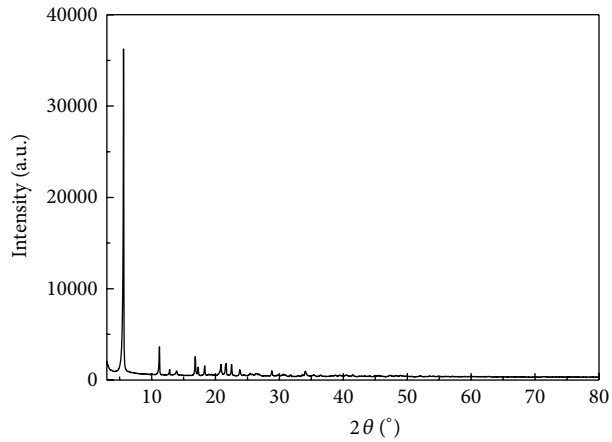

Figure 1: XRD pattern of the complex $Mn(HMHA)_2$.

3.3. IR Spectroscopy Analysis. The IR spectrum of the complex is shown in Figure 2. The peaks at 2914, 1438, and 1313 cm^{-1} are attributed to the characteristic absorption peaks of the CH_3S– group. The moderate intensity broad peak at 3434 cm^{-1} is attributed to the stretching vibration absorption peak of the –OH group between 3650 and 3200 cm^{-1}, and the characteristic stretching vibration absorption peak originated from the C–O bond of the secondary alcohols can be found at 1071 cm^{-1}, so we can infer that the –OH group participates in the coordination with metal ion. The absorption peaks at 1633 and 1578 cm^{-1} and 1383 cm^{-1} are attributed, respectively, to the antisymmetric and symmetric stretching vibration of the COO^- group. The difference values between $\nu_{as}(COO^-)$ and $\nu_s(COO^-)$ are 250 and 195 cm^{-1}, which is a sign that the carboxyl oxygen atoms are coordinated with manganese ion by the bridging coordination mode [10]. As shown in the spectrum, there are two strong absorption peaks near 1600 cm^{-1}, which are in accord with the absorption peaks at 1637 and 1580 cm^{-1} of the zinc complex of H_2MHA without water molecule [6]. The result illustrates that there is not any water molecule in the manganese complex of H_2MHA, and it is in line with the thermal decomposition process. In the low-frequency region, the absorption peaks at 572, 500, and 445 cm^{-1} in the complex are assigned to the stretching vibration of the Mn–O bond. In conclusion, the six oxygen atoms from two $HMHA^-$ anionic ligands are directly coordinated to the manganese ion, which should exhibit hexacoordination as occurs for the corresponding Mn^{2+} glycolate complex [11].

3.4. Thermal Decomposition Mechanism. Studying thermal decomposition process of complexes is helpful in the understanding of the coordination structure of the complexes

Table 2: Experimental data and calculated results for X-ray powder diffraction pattern of the complex $Mn(HMHA)_2$.

Number	$2\theta/(^\circ)$	h	k	l	d_{exp}/nm	d_{cal}/nm	I/I_0
1	5.615	0	0	1	1.5726	1.5724	100
2	11.217	0	2	0	0.7882	0.7882	8.7
3	12.804	1	0	−2	0.6908	0.6913	1.7
4	13.907	2	0	0	0.6363	0.6371	1.3
5	16.846	0	3	0	0.5259	0.5255	5.8
6	17.280	2	0	−2	0.5127	0.5131	2.6
7	18.309	1	3	0	0.4846	0.4858	2.9
8	18.965	1	3	−1	0.4676	0.4677	0.3
9	19.366	2	1	2	0.4580	0.4581	0.3
10	20.855	3	0	0	0.4256	0.4248	3.4
11	21.627	3	1	0	0.4106	0.4101	3.5
12	22.503	0	4	0	0.3948	0.3941	3.4
13	23.827	1	1	−4	0.3731	0.3725	1.8
14	24.487	3	0	2	0.3632	0.3631	0.3
15	25.379	2	2	3	0.3507	0.3506	0.7
16	25.772	2	0	−4	0.3454	0.3457	0.4
17	26.407	1	4	2	0.3372	0.3368	0.6
18	26.771	1	2	4	0.3327	0.3337	0.6
19	28.816	1	3	−4	0.3096	0.3097	1.6
20	29.882	3	3	2	0.2988	0.2987	0.4
21	30.332	3	1	−4	0.2944	0.2940	0.4
22	30.690	2	0	−5	0.2911	0.2903	0.6
23	30.987	4	0	2	0.2884	0.2882	0.4
24	31.754	3	4	1	0.2816	0.2817	0.6
25	32.930	2	2	−5	0.2718	0.2724	0.2
26	33.594	1	5	−3	0.2666	0.2663	0.6
27	34.059	3	2	4	0.2630	0.2629	1.5
28	35.371	1	6	1	0.2536	0.2534	0.5
29	36.490	0	5	−4	0.2460	0.2460	0.4
30	38.285	0	6	−3	0.2349	0.2349	0.3
31	38.768	4	0	−5	0.2321	0.2322	0.3
32	39.439	1	3	6	0.2283	0.2281	0.3
33	39.865	5	2	−3	0.2260	0.2260	0.2
34	40.538	0	1	7	0.2224	0.2224	0.4
35	41.485	1	5	5	0.2175	0.2175	0.5
36	43.360	3	2	6	0.2085	0.2086	0.2
37	44.085	5	0	−5	0.2053	0.2052	0.3
38	45.485	4	5	−4	0.1993	0.1990	0.5
39	47.266	1	0	8	0.1922	0.1922	0.4
40	48.169	5	5	−3	0.1888	0.1889	0.3
41	48.961	3	5	−6	0.1859	0.1860	0.4
42	52.047	5	6	−3	0.1756	0.1755	0.3
43	56.053	4	6	−6	0.1639	0.1639	0.2
44	57.115	3	7	−6	0.1611	0.1611	0.3
45	60.051	7	1	−6	0.1539	0.1540	0.2
46	66.347	2	9	6	0.1408	0.1408	0.2

[12, 13]. The TG-DTA curves of the complex of H_2MHA from room temperature to 600°C with a heating rate of 10°C min^{-1} are shown in Figure 3, and the TG and the DTG curves

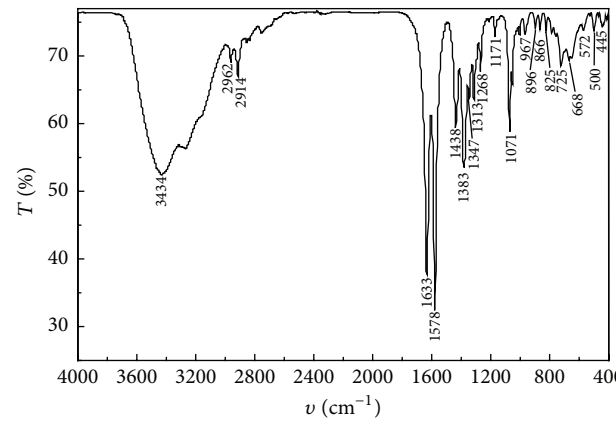

Figure 2: FTIR spectrum of the complex $Mn(HMHA)_2$.

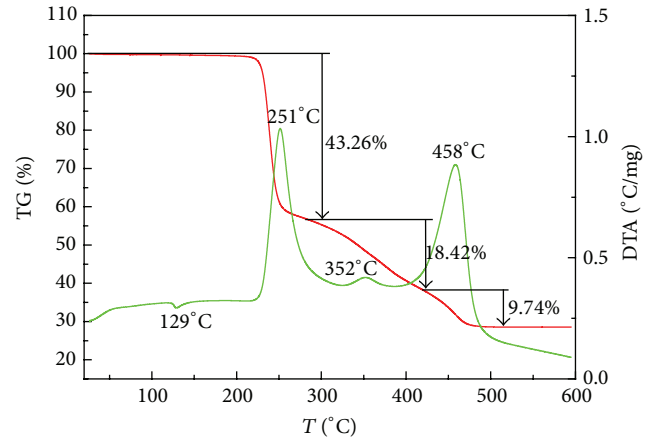

Figure 3: TG and DTA curves of the complex $Mn(HMHA)_2$.

of the complex at the heating rates of 5, 10, 15, and 20°C min^{-1} are presented in Figure 4. We can come to the conclusion from Figures 3 and 4 that the thermal decomposition process of the complex consists of three stages. With the increasing of the heating rate, the DTG curves move to the high temperature and the decomposition peak temperature T_p of every stage is also moving in the direction of high temperature [14]. This reveals that the change of the heating rate has a slight influence on the temperature range of each mass loss stage. In the first stage, the percentage of mass loss at different heating rates is basically unchanged. But the final residual mass of the thermal decomposition for the complex is decreased with the increasing of the temperature. The percentage of the residual mass at the heating rate of 15°C min^{-1} is 24.60%, and it is in good agreement with the theoretical calculated value of the residue of manganese sulfide in 24.62%. Figure 3 shows that the complex is stable in the air and is decomposed over 200°C, and its thermal stability is very good. The final residue is black and stable powder after the complex undergoes three consecutive mass loss stages. Figure 3 shows that there are one endothermic peak and three exothermic peaks in the DTA curve. First, there is a very weak endothermic peak at 129°C, while there

Table 3: Calculated results for the complex kinetic parameters of thermal decomposition using Kissinger and F-W-O methods.

Reaction stage	E/kJ mol^{-1}			r		ln A/s^{-1}
	Kissinger	F-W-O	Average	Kissinger	F-W-O	Kissinger
1	238.13	234.53	236.33	0.9986	0.9987	60.312
3	176.78	179.62	178.20	0.9891	0.9904	32.468

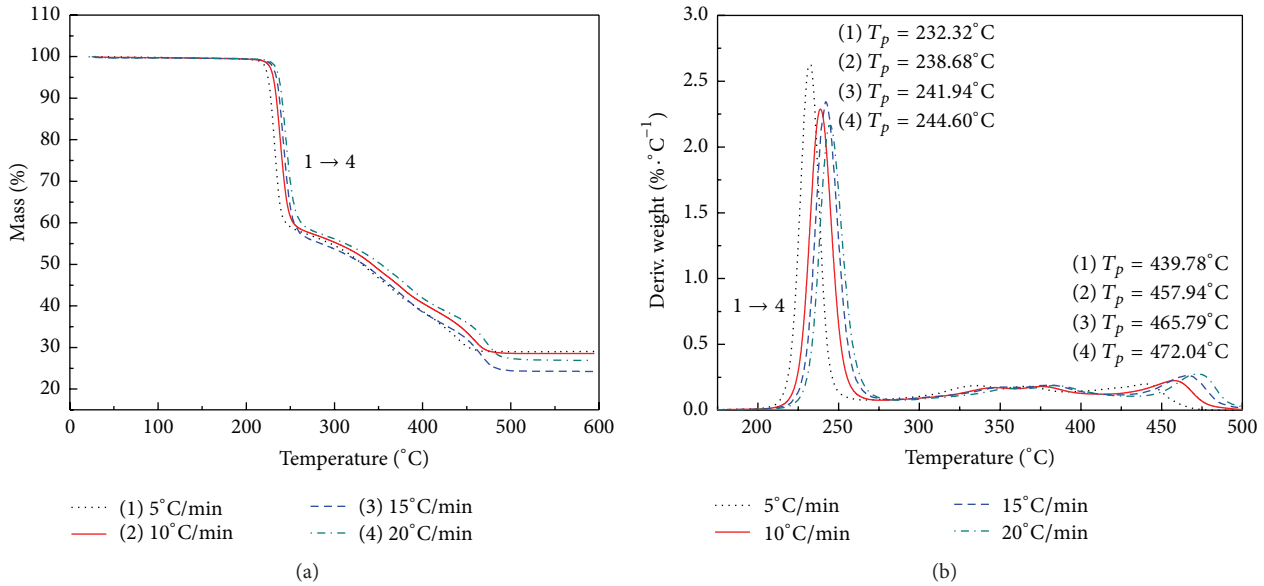

Figure 4: TG (a) and DTG (b) curves of the complex $Mn(HMHA)_2$ at different heating rates.

is no mass loss in the TG curve, and it is a melting and endothermic process of the complex of H_2MHA. At the first mass loss stage, there is a sharp exothermic peak at 251°C in the DTA curve, and it is ascribed to the oxidative decomposition of the ligand and the loss of one H_2MHA molecule $CH_3SCH_2CH_2CH(OH)COOH$. The experimental percentage mass loss of 43.26% in the TG curve is close to the calculated result of 42.51%. At this time, the title complex is transformed into the complex [Mn(MHA)] of the chelate ratio of 1 : 1. At the second and the third mass loss stages, there are one very weak exothermic peak at 352°C and one strong exothermic peak at 458°C in the DTA curve, and it is considered to be the oxidation and decomposition of the deprotonated MHA^{2-} ligand. The percentage of the residual mass in the TG curve is 28.58%, and there is some difference in the theoretical residual mass of 24.62% of manganese sulfide. It can be explained that partial manganese sulfide is oxidized to produce manganese sulfate when the heating rate is low.

3.5. Thermal Decomposition Kinetics Analysis. In order to obtain the thermal decomposition kinetic parameters of the title complex, two different dynamic analysis methods, namely, the Kissinger method and the Flynn-Wall-Ozawa (F-W-O) method, which are utilized to calculate the activation energy E, the preexponential factor A, and the correlation coefficient r at the first and the third mass loss stages of the complex, and the related results are shown in Figures 5 and 6 and Table 3. The basic equations of the Kissinger method [15–17] and the F-W-O method [18–21] are as follows:

$$\ln \frac{\beta}{T_p^2} = \ln \frac{AR}{E} - \frac{E}{RT_p}$$
$$\ln \beta = \lg \frac{AE}{RG(\alpha)} - 2.315 - 0.4567 \frac{E}{RT}, \quad (1)$$

where β is the heating rate (K min^{-1}), A is the preexponential factor (s^{-1}), R is the gas molar constant (8.314 J K^{-1} mol^{-1}), E is the activation energy (kJ mol^{-1}), α is the conversion rate (%), T_p is the thermal spectrum peak temperature of different heating rates (K), and $G(\alpha)$ is the integral mechanism function. Both of the two methods require several kinetic curves to perform the analysis and thus are sometimes called multicurve methods [22].

The Kissinger method is a model-free method, but it is not isoconversional method because it assumes constant activation energy with the progress of conversion instead of calculating activation energy at different constant extents of conversion [23]. According to Kissinger, the maximum reaction rate occurs with an increase in the reaction temperature [16]. As shown in Figures 5(a) and 6(a), the plot of $\ln(\beta/T_p^2)$ versus $1/T_p$ obtained from thermal curves recorded at different heating rates is a straight line whose slope can be used to calculate the activation energy E and the intercept can be used to calculate the preexponential factor A. In the F-W-O method, when the percentage mass loss of the complex

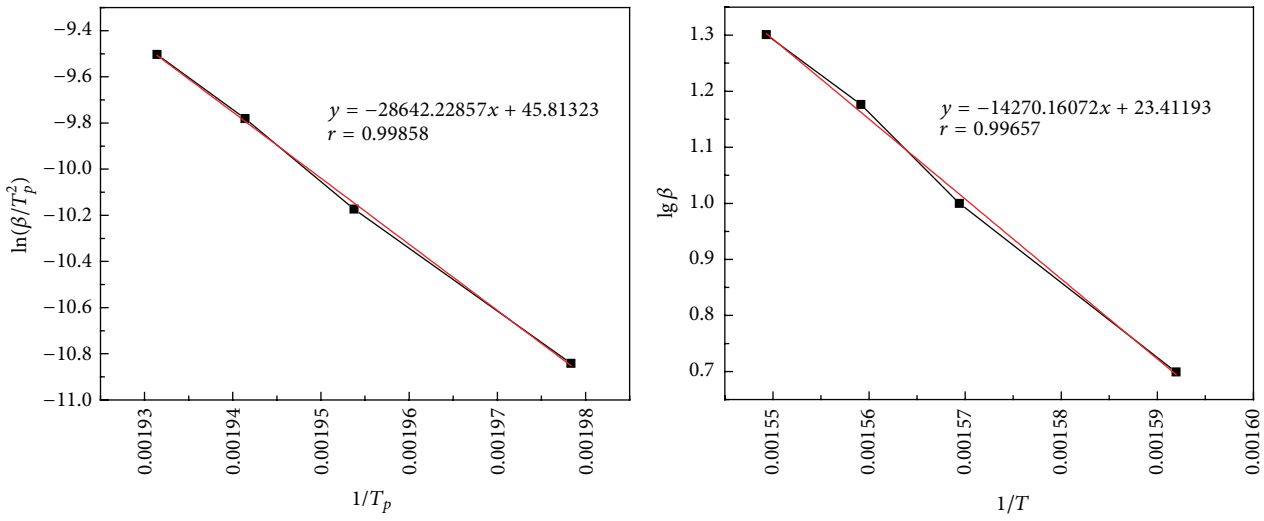

(a) Curve of $\ln(\beta/T_p^2)$ versus $1/T_p$ (b) Curve of $\lg\beta$ versus $1/T$

Figure 5: Linear relationship at different heating rates and T_p for the first stage.

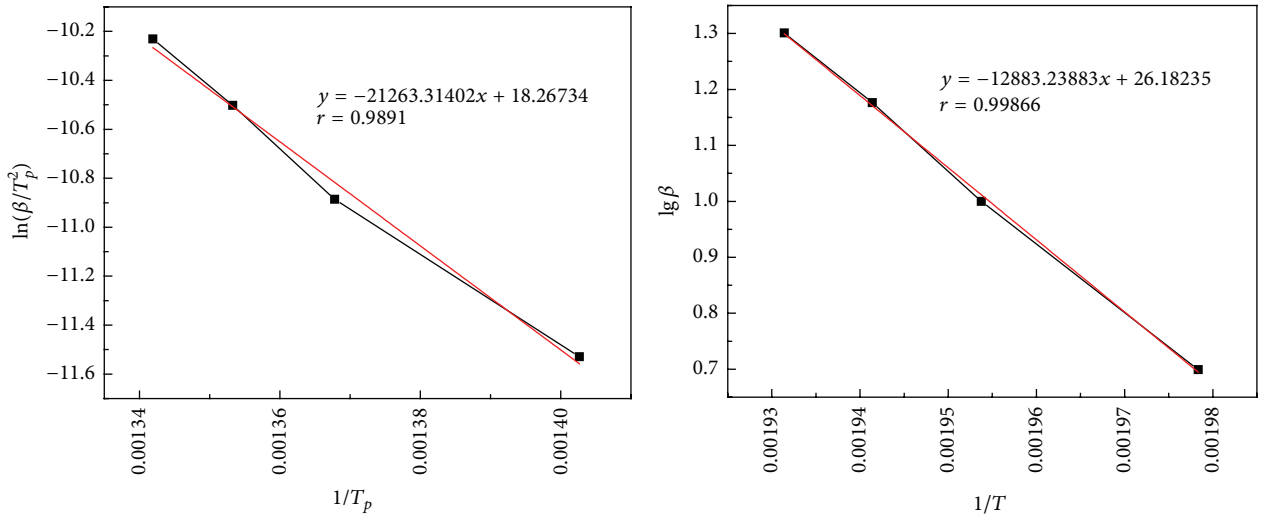

(a) Curve of $\ln(\beta/T_p^2)$ versus $1/T_p$ (b) Curve of $\lg\beta$ versus $1/T$

Figure 6: Linear relationship at different heating rates and T_p for the third stage.

in different heating rates β is 20% at the thermal spectrum peak temperature T_p, the conversion rate α is approximately equal. The activation energy can be obtained from the plot of $\lg\beta$ versus $1/T_p$ for a series of experiments at different heating rates, the data of which are linearly fitted by least square method, and the results are exhibited in Figures 5(b) and 6(b). From Table 3, the activation energy of the pyrolysis of the complex obtained by the Kissinger method is extremely close to the one by the F-W-O method.

There are various possibilities to express the conversion function for the solid-state reactions. Most of the previous authors used the conversion function, namely, $f(\alpha) = (1-\alpha)^n$. The equation which can be obtained by the Freeman-Carroll method [24–26] is as follows:

$$\ln\frac{d\alpha}{dt} + \frac{E}{RT} = \ln A + n\ln(1-\alpha). \quad (2)$$

The average value of the activation energy obtained from the above two methods is used as the activation energy of the thermal decomposition processes. The preexponential factor A can be obtained by Kissinger and Freeman-Carroll methods. As shown in Figure 7, according to the thermal decomposition data with a heating rate of $5^\circ\mathrm{C\,min^{-1}}$, the plot of $\ln(d\alpha/dt)+E/RT$ versus $\ln(1-\alpha)$ is obtained in the first and

Table 4: Calculated results for the complex kinetic parameters using Kissinger and Freeman-Carroll methods.

Reaction stage	$\ln A/s^{-1}$			r		n
	Kissinger	Freeman-Carroll	Average	Kissinger	Freeman-Carroll	Freeman-Carroll
1	60.312	54.034	57.173	0.9986	0.9706	0.91
3	32.468	27.187	29.828	0.9891	0.9543	0.91

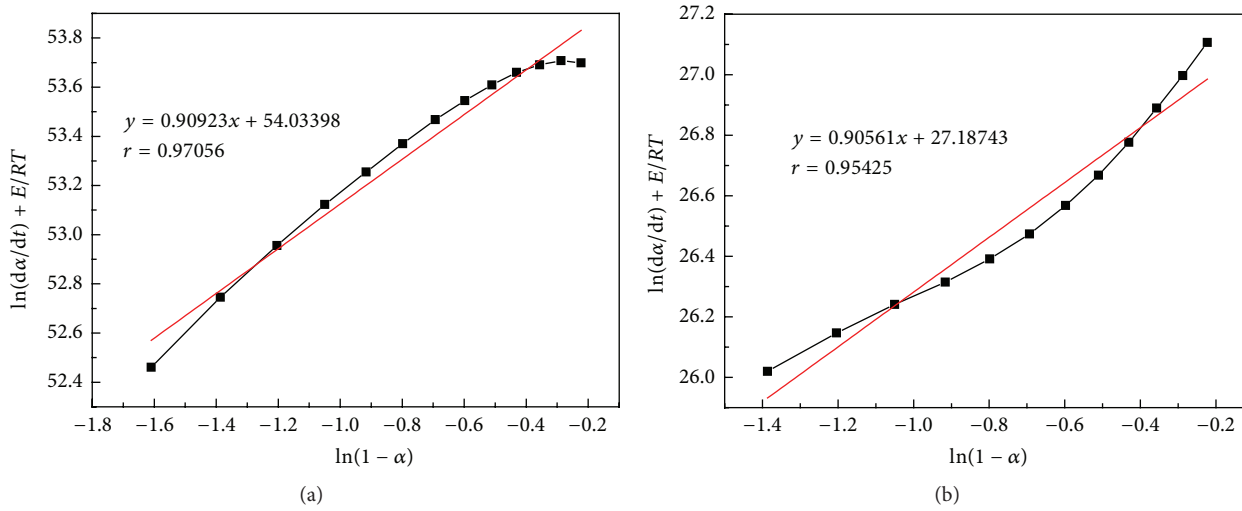

Figure 7: Curves of $\ln(d\alpha/dt) + E/RT$ versus $\ln(1-\alpha)$ at the first (a) and the third (b) stages of the thermal decomposition.

the third mass loss stages. The reaction order can be found out through the slope of the line, and the preexponential factor A can be gotten by the intercept. The results are displayed in Table 4. The kinetic equation for the thermal decomposition of the title complex can be obtained by the nonisothermal kinetic equation [17]:

$$\frac{d\alpha}{dt} = A\left[\exp\left(-\frac{E}{RT}\right)\right](1-\alpha)^n. \quad (3)$$

The thermal decomposition kinetic parameters of E, A, and n are substituted into (3), and the thermal decomposition kinetics equations of the title complex in the first and the third mass loss stages can be obtained as follows:

$$\frac{d\alpha}{dt} = 6.760 \times 10^{24}\left[\exp\left(-\frac{236.33\times10^3}{RT}\right)\right](1-\alpha)^{0.91}$$
$$\frac{d\alpha}{dt} = 8.998 \times 10^{12}\left[\exp\left(-\frac{178.20\times10^3}{RT}\right)\right](1-\alpha)^{0.91}. \quad (4)$$

4. Conclusion

The manganese complex of H_2MHA was synthesized with DL-2-hydroxy-(4-methylthio) butanoic acid and manganese chloride as main raw materials, and the complex was characterized by elemental analyses, FTIR, XRD, and TG-DTA-DTG. The index results of the XRD data show that the crystal structure of the complex belongs to monoclinic system with the cell parameters of a = 1.2775 nm, b = 1.5764 nm, c = 1.5764 nm, and β = 94.06°. The Mn(II) ion is hexacoordinated by the carboxylic and hydroxyl oxygen atoms from the H_2MHA ligand. The thermal decomposition processes of the complex in the air illustrate that the complex is stable at room temperature and is decomposed over 200°C, and the final residue is mainly manganese sulfide. The thermal decomposition kinetics equations and parameters of the complex in the first and the third mass loss stages are obtained by nonisothermal kinetic theory and dynamic methods. The results are as follows: the activation energy E is 236.33 and 178.20 kJ mol^{-1}, the reaction order n is 0.91 and 0.91, and the preexponential factor $\ln(A)$ is 57.173 and 29.828, respectively.

Conflict of Interests

The authors declare that there is no conflict of interests regarding the publication of this paper.

Acknowledgments

This work was supported by the Scientific Research Funds of Education Department of Sichuan Province (10ZA016). The authors are very grateful to Analytical and Testing Center of Southwest University of Science and Technology and Engineering Research Center of Biomass Materials of Education Ministry for the testing of elemental analyses, XRD, FTIR, and TG-DTG-DTA.

References

[1] G. Predieri, M. Tegoni, E. Cinti, G. Leonardi, and S. Ferruzza, "Metal chelates of 2-hydroxy-4-methylthiobutanoic acid in animal feeding: preliminary investigations on stability and bioavailability," *Journal of Inorganic Biochemistry*, vol. 95, no. 2-3, pp. 221–224, 2003.

[2] Q. J. Sun, Y. M. Guo, T. G. Zhang, and J. L. Wen, "Effects of 2-hydroxy-4-(methylthio)-butanoic acid chelated Cu/Mn/Zn on eggshell quality, enzyme activity and trace mineral retention in laying hens," *Journal of China Agricultural University*, vol. 16, no. 4, pp. 127–133, 2011.

[3] G. Predieri, L. Elviri, M. Tegoni et al., "Metal chelates of 2-hydroxy-4-methylthiobutanoic acid in animal feeding: part 2: further characterizations, in vitro and in vivo investigations," *Journal of Inorganic Biochemistry*, vol. 99, no. 2, pp. 627–636, 2005.

[4] European Food Safety Authority, "Scientific opinion of the panel on additives and products or substances used in animal feed-safety and efficacy of mintrex Cu (copper chelate of hydroxy analogue of methionine) as feed additive for all species," *The EFSA Journal*, vol. 693, p. 2, 2008.

[5] Z.-X. Wu, C.-C. Li, G.-Q. Zhong, D. Li, M. Tao, and W.-X. Zhang, "Preparation and characterization of copper chelate of hydroxymethionine," *Journal of Synthetic Crystals*, vol. 43, no. 2, pp. 474–479, 2014.

[6] G. Predieri, D. Beltrami, R. Pattacini et al., "Structural studies in solution and in the solid state on the zinc chelate of 2-hydroxy-(4-methylthio)butanoic acid, an effective mineral supplement in animal feeding," *Inorganica Chimica Acta*, vol. 362, no. 4, pp. 1115–1121, 2009.

[7] H. B. Xu, K. H. Cheng, D. D. Shi, and W. Wang, "Progress of synthesis of 2-hydroxy-4-(methylthio) butyric acid and its calcium salt," *Progress in Modern Biomedicine*, vol. 9, no. 7, pp. 1387–1389, 2009.

[8] G.-Q. Zhong, Y.-C. Guo, Y.-R. Chen, X.-S. Zang, and S.-R. Luan, "Synthesis and crystal structure of the complex of thioglycollic acid and trivalent antimony ion," *Acta Chimica Sinica*, vol. 59, no. 10, pp. 1599–1603, 2001.

[9] D. Li and G.-Q. Zhong, "Synthesis and crystal structure of the bioinorganic complex $[Sb(Hedta)]\cdot 2H_2O$," *Bioinorganic Chemistry and Applications*, vol. 2014, Article ID 461605, 7 pages, 2014.

[10] G. B. Deacon and R. J. Phillips, "Relationships between the carbon-oxygen stretching frequencies of carboxylato complexes and the type of carboxylate coordination," *Coordination Chemistry Reviews*, vol. 33, no. 3, pp. 227–250, 1980.

[11] G. G. Melikyan, F. Amiryan, M. Visi et al., "Manganese(II)/(III) glycolates: preparation, X-ray crystallographic study, and application in radical cycloaddition reactions," *Inorganica Chimica Acta*, vol. 308, no. 1-2, pp. 45–50, 2000.

[12] G. Q. Zhong, J. Shen, Q. Y. Jiang, Y. Q. Jia, M. J. Chen, and Z. P. Zhang, "Synthesis, characterization and thermal decomposition of Sb^{III}-M-Sb^{III} type trinuclear complexes of ethylenediamine-N, N, N′, N′-tetraacetate (M: Co(II), La(III), Nd(III), Dy(III))," *Journal of Thermal Analysis and Calorimetry*, vol. 92, no. 2, pp. 607–616, 2008.

[13] X. Liu, N. Liu, and Y. Zhang, "Synthesis, characterization, scavenging free radical and bacteriostasis characteristics of calcium-genistein complex," *CIESC Journal*, vol. 61, no. 11, pp. 3006–3013, 2010.

[14] N. Punsuwan and C. Tangsathitkulchai, "Product characterization and kinetics of biomass pyrolysis in a three-zone free-fall reactor," *International Journal of Chemical Engineering*, vol. 2014, Article ID 986719, 10 pages, 2014.

[15] L.-Q. Duan, C.-F. Qiao, Q. Wei et al., "Structures, thermodecomposition kinetics and luminescence properties of three lanthanide-based supramolecular compounds with 1H-benzimidazole-2-carboxylic acid," *Acta Physico—Chimica Sinica*, vol. 28, no. 12, pp. 2783–2789, 2012.

[16] H. E. Kissinger, "Reaction kinetics in differential thermal analysis," *Analytical Chemistry*, vol. 29, no. 11, pp. 1702–1706, 1957.

[17] L. Cheng, B. L. Zhang, L. Xu, C. H. Hou, and G. J. Liu, "Thermal decomposition kinetics of humic acid," *CIESC Journal*, vol. 65, no. 9, pp. 3470–3478, 2014.

[18] R. Z. Hu, S. L. Gao, F. Q. Zhao, Q. Z. Shi, T. L. Zhang, and J. J. Zhang, *Thermal Analysis Kinetics*, Science Press, Beijing, China, 2nd edition, 2008.

[19] D. Zhan, C. J. Cong, K. Diakite, Y. T. Tao, and K. L. J. Zhang, "Kinetics of thermal decomposition of nickel oxalate dihydrate in air," *Thermochimica Acta*, vol. 430, no. 1-2, pp. 101–105, 2005.

[20] S. M. Pourmortazavi, I. Kohsari, M. B. Teimouri, and S. S. Hajimirsadeghi, "Thermal behaviour kinetic study of dihydroglyoxime and dichloroglyoxime," *Materials Letters*, vol. 61, no. 25, pp. 4670–4673, 2007.

[21] J. Zsakó, "Kinetic analysis of thermogravimetric data," *The Journal of Physical Chemistry*, vol. 72, no. 7, pp. 2406–2411, 1968.

[22] J. H. Flynn and L. A. Wall, "General treatment of the thermogravimetry of polymers," *Journal of Research of the National Bureau of Standards Section A: Physics and Chemistry*, vol. 70, no. 6, pp. 487–523, 1966.

[23] A. Khawam, *Application of solid-state kinetics to desolvation reactions [Ph.D. thesis]*, University of Iowa, Iowa City, Iowa, USA, 2007.

[24] E. S. Freeman and B. Carroll, "The application of thermoanalytical techniques to reaction kinetics: the thermogravimetric evaluation of the kinetics of the decomposition of calcium oxalate monohydrate," *The Journal of Physical Chemistry*, vol. 62, no. 4, pp. 394–397, 1958.

[25] P. Wang, X. Gong, B. Zhang, E. V. Leng, Z. G. Chen, and M. H. Xu, "Characteristics of cellulose from ionic liquid regeneration," *CIESC Journal*, vol. 65, no. 12, pp. 3799–4793, 2014.

[26] H.-W. Liao, Y.-M. Pan, and Y. Zhou, "Thermal decomposition kinetics of $[Sr(C_6H_4NO_2)_2 \cdot 3H_2O]$," *Journal of Chemical Engineering of Chinese Universities*, vol. 28, no. 3, pp. 472–476, 2014.